The Effect of Natural Flow of Aquifers and Associated Dispersion on the Onset of Buoyancy-Driven Convection in a Saturated Porous Medium

Hassan Hassanzadeh, Mehran Pooladi-Darvish, and David W. Keith
Dept. of Chemical and Petroleum Engineering, University of Calgary, Calgary, AB, Canada

DOI 10.1002/aic.11664
Published online December 17, 2008 in Wiley InterScience (www.interscience.wiley.com).

Carbon dioxide injection into deep saline aquifers is an important option for managing CO_2 emissions. Injected CO_2 dissolves into formation brines from above, increasing brine density and creating an unstable hydrodynamic state favorable for natural convection. Long-term buoyancy-driven flow of high-density CO_2-saturated brine leads to faster trapping through improved dissolution and can reduce the risk of CO_2 leakage from storage sites. We investigate the role of natural flow of aquifers and associated dispersion on the onset of convection. A linear stability analysis of a transient concentration field in a laterally infinite, horizontal, and saturated porous layer with steady horizontal flow is presented. The layer is subjected to a sudden rise in CO_2 concentration from the top and is closed from the bottom. Solution of the stability equations is obtained using a Galerkin technique and the resulting equations are integrated numerically. We found simple scaling relationships that follow $t_{Dc} \sim 60(1 + Pe_T)Ra^{-2}$ for the onset time of convection and $a \sim 0.05Ra/(1 + Pe_T)$ for the wavenumber of the initial instabilities. Results reveal that transverse dispersion increases the time to onset of convection for the entire range of Ra. Furthermore, transverse dispersion decreases the critical wavenumber of the instabilities. These results facilitate screening candidate sites for geological CO_2 storage. © 2008 American Institute of Chemical Engineers *AIChE J,* 55: 475–485, 2009

Keywords: convection, stability analysis, dispersion, saline aquifers, CO_2, storage or sequestration

Introduction

The modeling of buoyancy-driven flow has a wide range of applications in science and engineering. The effect of dispersion on convective mixing of fluids in a porous medium is important for various applications, including CO_2 storage, groundwater motion, contaminant migration, and petroleum and geothermal reservoirs. The problem of stability analysis for clear fluids (i.e., not within a porous medium) under various boundary conditions has been reported in the literature.[1–11] Investigation of the stability analysis of a fluid in a saturated porous medium can be divided into two categories. The first category is one with an initially stationary fluid in a porous medium; the second category is one with an initially nonstationary fluid in a porous medium. The problem of hydrodynamic stability of an initially stationary fluid in a porous medium has been studied extensively in the literature for various boundary conditions under steady-state and transient

Correspondence concerning this article should be addressed to M. Pooladi-Darvish at pooladi@ucalgary.ca.

temperature or concentration fields.[12–21] Different methods have been used to study stability of time dependent concentration or temperature profiles including linear amplification theory,[3,6] the energy method,[22] the nonlinear amplitude method,[23] maximum transient Rayleigh number theory,[11] and the propagation theory.[24] It has been reported that the onset time predicted by the energy method is almost one order of magnitude less than actual measured laboratory data,[9] whereas the linear amplification theory gives values that more closely agree with the experimental values.[3,6,20] Kaviany[20] investigated the onset of thermal convection in a porous medium both theoretically and experimentally. Kim et al.,[25] Kim et al.,[26] and Kim and Kim[27] studied the onset of buoyancy-driven flow in a porous medium without basic flow. Ennis-King and Paterson[28] Ennis-King et al.[29] and Hong and Kim[30] performed a linear stability analysis to investigate the role of permeability anisotropy on the onset of convection. Riaz et al.[31] used linear stability analysis based on the dominant mode of the self-similar diffusion operator and found a scaling relationship for the onset of convection. Xu et al.[32] used linear stability analysis to find the onset of convection. Hassanzadeh et al[33] studied the effect of various boundary conditions on the onset of convection in a porous medium.

All of the aforementioned works assume an initially stationary fluid in a porous medium under a variety of boundary conditions. For cases where the fluid in the porous medium is initially flowing, local variations in concentration and temperature gradients may be introduced through the use of the concept of hydrodynamic dispersion.[34] It is known that the magnitude of the hydrodynamic dispersion is an increasing function of the pore scale Peclet number, where Peclet number is directly related to the fluid velocity.[34] The role of hydrodynamic dispersion on the stability of an initially nonstationary fluid in a porous medium with steady-state temperature or concentration fields has also been studied by many investigators.[35–46] Previous studies have shown that natural flow of aquifers and associated transverse dispersion retard the convection for a nonstationary fluid in a porous medium with linear temperature or concentration fields.[39–42] However, none of the previous works quantified the role of natural flow of aquifers and associated dispersion on the onset of convection for transient temperature or concentration profiles, despite the fact that for practical problems such as the dissolution of CO_2 injected into aquifers are transient. Our objective in this article is to understand how background flow in aquifers can modify the onset of convection in a transient concentration field by deriving a time scale for the onset of convection as a function of the velocity of background flow.

Finally, we show that natural flow of aquifer and associated dispersion can substantially increase the time scale for convectively driven dissolution of CO_2 in aquifer brines. Slowing the rate of dissolution is important because it prolongs the duration over which buoyant free-phase CO_2 is present in an aquifer, increasing the possibility that CO_2 could migrate upwards perhaps leaking to the surface.

The Physical Problem

The CO_2 injected into a saline aquifer is less dense than the resident brine. Driven by density contrasts, CO_2 will therefore flow up and then horizontally (in a horizontal aquifer), spreading under the cap rock, and will flow upwards leaking through any high permeability zones or artificial penetrations such as abandoned wells with poor cement integrity. The free-phase CO_2 (gas or, more typically, supercritical fluid) slowly dissolves and diffuses into the formation brine. Dissolution of most gases in water decreases the fluid density. However, CO_2 is one of the few gases for which dissolution increases fluid density.[47–50] This increase in density is the driver for convective dissolution of CO_2 injected into brine-filled aquifers.

The diffusion of CO_2 near the top of the aquifer into formation brine at that location increases the density of brine, bringing the system to a hydro-dynamically unstable state. Instabilities can arise from the combination of an unstable density profile and inherent perturbations within the system. Such instabilities, if created, cause convective mixing and greatly accelerate the dissolution of CO_2 into the aquifer.[28,51,52] The dissolution process has a timescale on many centuries. In previous work, for example, we have shown that in the Nisku aquifer in the Alberta basin dissolution of CO_2 by pure diffusion will take thousands of years whereas convective mixing can dissolve 60% of CO_2 in 800 years.[52] Although the CO_2 remains in the undissolved free phase, there is a risk of leakage arising from strong buoyancy driven flow. Assessments of the risk of leakage of CO_2 from a storage formation may need to consider leakage mechanisms and their likelihood of occurrence during the full time period over which mobile free-phase CO_2 is expected to remain in the reservoir. Convective mixing increases the rate of dissolution and therefore decreases the timescale (i.e., decreases the likelihood) over which leakage is possible. Once CO_2 is dissolved, risk assessments may well ignore the leakage pathways resulting from the very slow movement of CO_2-saturated brines. Therefore, developing suitable criteria for the onset of convection is important in the design and implementation of large-scale geological CO_2 storage in saline aquifers.[53] Natural flow in aquifers and dispersion might influence the onset of such convective mixing. This article provides the first investigation of the role of natural flow of aquifers and associated dispersion on the onset of buoyancy-driven convection in a porous medium when a time-dependent concentration field exists.

The remainder of this article is organized as follows. First, the governing equations are described. Then a linear stability analysis is presented, followed by a methodology to determine the onset of convection. After that, results of the analysis are presented and discussed. Then, we provide an application of the results for a number of Alberta basin aquifers. Finally, limitations of the analysis presented are described, followed by conclusions.

Theoretical Analysis

Governing equations

The physical model and the coordinate system used in this study are shown in Figure 1. The model is a porous medium with thickness H saturated with brine and closed from the bottom. The lateral extent is infinite and brine flows through the porous medium with a constant background velocity U. The saturated porous medium has a constant porosity ϕ and

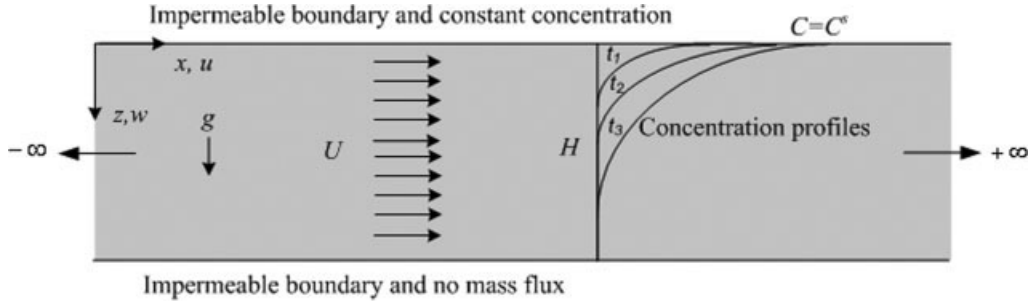

Figure 1. A schematic of the problem showing boundary conditions.

permeability k. The domain that is initially free of CO_2 is rapidly exposed to a constant CO_2 concentration from the top at time zero, leading to diffusion and increased density at the top of the formation. It is well known that such a top-heavy arrangement is unstable when the Rayleigh number exceeds a certain critical value. The Darcy model and Boussinesq approximation[54] are assumed valid. For such a system, the governing equations of flow and concentration field are expressed by:

$$\nabla \cdot \mathbf{v} = 0, \tag{1}$$

$$\mathbf{v} = -\frac{k}{\mu}(\nabla p - \rho g \nabla z), \tag{2}$$

$$\phi K \nabla^2 C - \mathbf{v} \cdot \nabla C = \phi \frac{\partial C}{\partial t}, \tag{3}$$

$$\rho = \rho_r(1 + \beta C), \tag{4}$$

where $\mathbf{v}$ is the Darcy velocity vector, p is pressure, C is concentration, μ and ρ are brine viscosity and density, respectively, β is the coefficient of density increase, K is the dispersion tensor, and subscripts r denotes reference.

The dispersion tensor for flow in an isotropic medium can be written as[39]:

$$K_{ij} = D\delta_{ij} + \frac{(\alpha_l - \alpha_t)}{\phi|\mathbf{v}|}\mathbf{v}_i\mathbf{v}_j + \alpha_t \frac{|\mathbf{v}|}{\phi}\delta_{ij}, \tag{5}$$

where δ is the Kronecker delta, $\mathbf{v}$ is the Darcy velocity, D is the molecular diffusion coefficient, and α_l and α_t are the longitudinal and transverse dispersivity, respectively.[34] Dispersivities are often said to represent the effect of spatially unresolved mixing because of pore-scale flow. In practice, dispersivities may also represent mixing because of flow through inhomogeneous media where the spatial scale of the inhomogeneity is smaller that the scale of measurement or numerical simulation. Dispersion coefficient K, is usually obtained from measurements of concentration breakthrough curves. Sternberg presented details for measurements of dispersion coefficient in porous media.[55]

The stability of such a system is characterized by the value of a dimensionless group (Ra) given by[12,13]:

$$Ra = \frac{k\Delta\rho g H}{\mu\phi D} \tag{6}$$

where $\Delta\rho = C^s\rho_r\beta$ and C^s is the top boundary concentration. As we shall see, Ra is a key dimensionless group determining the stability behavior of the system.

We define a set of dimensionless variables C_{0D}, z_D, t_D by using the scale of concentration C^s, length H, and time H^2/D. Then the base state can be expressed by:

$$(1 + \mathrm{P}_{e_T})\frac{\partial^2 C_{0D}}{\partial z_D^2} = \frac{\partial C_{0D}}{\partial t_D}, \tag{7}$$

where the base state is defined by $C = C_0$, $u_0 = U$, $v_0 = 0$, and $w_0 = 0$ and The dimensionless group P_{e_T} is the transverse Peclet number given by:

$$\mathrm{P}_{e_T} = \frac{\alpha_t U}{D\phi}. \tag{8}$$

The initial condition is given by $C_{0D} = 0$. The boundary conditions at $z_D = 0$ and $z_D = 1$ for the base state are expressed by $C_{0D} = 1$ and $\partial C_{0D}/\partial z_D = 0$, respectively. The analytical solution for the base solution can be obtained by separation of variables and is given by[56]:

$$C_{0D} = 1 - \frac{4}{\pi}\sum_{n=1}^{\infty}\frac{1}{(2n-1)}\sin\left(\frac{(2n-1)}{2}\pi z_D\right) \times \exp\left(-\left(\frac{2n-1}{2}\right)^2 \pi^2(1 + \mathrm{P}_{e_T})t_D\right). \tag{9}$$

In this work, we quantify the effect of dispersion on instability based on the magnitude of P_{e_T} as a measure of dispersion. In the following, we follow previous works of Foster,[3,6] Kim and Kim,[27] Ennis-King and Paterson,[28] and Hassanzadeh et al.[33] to perform a linear stability analysis for this new problem of transient concentration field in the presence of background flow.

Stability Analysis

The base state concentration and velocity are subjected to an infinitesimal perturbation. The perturbed parameters can be expressed as $C = C_0 + C'$ and $\mathbf{v} = \mathbf{v}_0 + \mathbf{v}'$, where the primed parameters are the perturbation quantities. In terms of perturbation velocity field and at a high aquifer background velocity one may write:

$$|\mathbf{v}| = \sqrt{(U + u')^2 + v'^2 + w'^2} \cong U. \tag{10}$$

where u, v, and w are components of the velocity vector in x-, y-, and z-direction, respectively. The dispersion tensor elements in the perturbed velocity field are given by:

$$K_{xx} = D(1 + \mathrm{P}_{e\mathrm{L}}), \tag{11}$$

$$K_{yy} = K_{zz} = D(1 + \mathrm{P}_{e\mathrm{T}}), \tag{12}$$

where $\mathrm{P}_{e\mathrm{T}} = \alpha_t U/\phi D$ and $\mathrm{P}_{e\mathrm{L}} = \alpha_l U/\phi D$ are the transverse and longitudinal Peclet number, respectively.

If second-order nonlinear perturbations are neglected, one can show that the off-diagonal elements of the dispersion tensor in the perturbed velocity field are zero. Therefore, neglecting the second-order nonlinear perturbation quantities and noting that the base concentration distribution is only a function of time and the vertical coordinate (Eq. 9), the dimensionless form of the governing equations of the vertical velocity and concentration (Eqs. 1 and 3) in terms of perturbed quantities are given by:

$$\nabla^2 w'_D = Ra\nabla_1^2 C'_D, \tag{13}$$

$$\nabla^2 C'_D + \mathrm{P}_{e\mathrm{L}}\frac{\partial^2 C'_D}{\partial x_D^2} + \mathrm{P}_{e\mathrm{T}}\nabla_2^2 C'_D - U_D\frac{\partial C'_D}{\partial x_D} - w'_D\frac{\partial C_{0D}}{\partial z_D} = \frac{\partial C'_D}{\partial t_D}. \tag{14}$$

where $\nabla_1^2 = \partial^2/\partial x_D^2 + \partial^2/\partial y_D^2$ and $\nabla_2^2 = \partial^2/\partial y_D^2 + \partial^2/\partial z_D^2$; C'_D has scale C^s; w' and U_D (dimensionless aquifer background velocity) have scale $\phi D/H$; and x_D and y_D have scale H. The appropriate boundary conditions are no-flow boundaries at the top ($z_D = 0$) and bottom ($z_D = 1$) for the velocity equation as given by $w'_D = w_D = 0$ and $\partial^2 w'_D/\partial {z_D}^2 = \partial^2 w_D/\partial {z_D}^2 = 0$, respectively. The proper boundary conditions for concentration are constant concentration at the top and zero mass flux at the bottom as represented by $C'_D = 0$ and $\partial C'_D/\partial z_D = 0$, respectively.

Here we have made the customary assumption that the perturbed velocity and concentration can be expressed as[3]:

$$\begin{bmatrix} w'_D(t_D, x_D, y_D, z_D) \\ C'_D(t_D, x_D, y_D, z_D) \end{bmatrix} = \begin{bmatrix} w^*_D(t_D, z_D) \\ C^*{}_D(t_D, z_D) \end{bmatrix} \exp[i(a_x x_D + a_y y_D)], \tag{15}$$

where $a = (a_x^2 + a_y^2)^{1/2}$ is the horizontal wavenumber and i is the imaginary number. Introducing perturbed quantities given by Eq. 15 into Eqs. 13 and 14 gives a system of differential equations for the amplitude functions of velocity and concentration as given by:

$$(\mathrm{D}^2 - a^2)w^*_D = -a^2 Ra C^*_D, \tag{16}$$

$$[\mathrm{D}^2 - a^2 - \mathrm{P}_{e\mathrm{L}}a_x^2 + \mathrm{P}_{e\mathrm{T}}(\mathrm{D}^2 - a_y^2) - U_D i a_x]C^*_D(t_D, z_D) - w^*_D(t_D, z_D)\frac{\partial C_0}{\partial z_D} = \frac{\partial C^*_D}{\partial_D}, \tag{17}$$

where $\mathrm{D} = d/dz_D$.

Separating imaginary and real parts gives:

$$U_D i a_x C^*_D(t_D, z_D) = 0, \text{implyiing that } a_x = 0 \quad (\text{longitudinal rolls}). \tag{18}$$

Equation 18 suggests that the preferred mode consists of longitudinal rolls aligned along the natural flow of an aquifer.[39,40] Although in the absence of natural flow of an aquifer ($U = 0$), the convective cells behave like rolls rotating with an axis perpendicular to the x-direction, in the presence of the natural flow of an aquifer, the axis of rotation of the rolls becomes parallel to the direction of natural flow of an aquifer.

The real part of the concentration amplitude equation gives:

$$(1 + \mathrm{P}_{e\mathrm{T}})[\mathrm{D}^2 - a^2]C^*_D(t_D, z_D) - w^*_D(t_D, z_D)\frac{\partial C_0}{\partial z_D} = \frac{\partial C^*_D}{\partial t_D}. \tag{19}$$

By making use of the Galerkin technique, the amplitude functions are represented by a system of linearly independent functions satisfying the boundary conditions[3,6,27–29,32,33]:

$$w^*_D = \sum_{l=1}^{N} A_l(t_D)\sin(l\pi z_D), \tag{20}$$

$$C^*_D = \sum_{l=1}^{N} B_l(t_D)\sin\left(\frac{(2l-1)}{2}\pi z_D\right). \tag{21}$$

Introducing the aforementioned equations into the amplitude equations and using the orthogonality property gives:

$$E_{lm}A_l(t_D) = F_{lm}RaB_l(t_D), \tag{22}$$

$$W_{lm}\frac{dB_l}{dt_D} = R_{lm}B_l - J_{lm}A_m, \tag{23}$$

where

$$E_{lm} = \delta_{lm}\left((l\pi)^2 + a^2\right), \tag{24}$$

$$F_{lm} = \frac{8a^2 m(-1)^{m-l+1}}{\pi(-1 + 2l - 2m)(-1 + 2l + 2m)}, \tag{25}$$

$$W_{lm} = \delta_{lm}, \tag{26}$$

$$R_{lm} = -\delta_{lm}(1 + \mathrm{P}_{e\mathrm{T}})\left(\left(\frac{(2l-1)\pi}{2}\right)^2 + a^2\right), \tag{27}$$

$$J_{lm} = 2\int_0^1 \frac{\partial C_{0D}}{\partial z_D}\sin(l\pi z_D)\sin\left(\frac{(2m-1)\pi z_D}{2}\right)dz_D, \tag{28}$$

where δ_{lm} is the Kronecker delta and E, F, W, J, and R are N by N matrices.

It can be shown that:

$$J_{lm} = \left[\exp\left(-\left(\frac{(2(m-l)-1)}{2}\right)^2\pi^2(1 + \mathrm{P}_{e\mathrm{T}})t_D\right) - \exp\left(-\left(\frac{2(l+m)-1}{2}\right)^2\pi^2(1 + \mathrm{P}_{e\mathrm{T}})t_D\right)\right]. \tag{29}$$

Using Eqs. 22 and 23 and eliminating $A_l(t_D)$ results in:

$$\frac{dB_l(t_D)}{dt_D} = G_{lm}B_l(t_D), \tag{30}$$

where $\boldsymbol{G}$ is an $\mathbf{N}$ by $\mathbf{N}$ matrix expressed by:

$$G_{lm} = \mathbf{W}^{-1}[\mathbf{R} - Ra\mathbf{J}\mathbf{E}^{-1}\mathbf{F}]. \quad (31)$$

The system of $\mathbf{N}$ ordinary differential equations given by Eq. 30 can be solved numerically using standard methods. Because the evolved convective instabilities appear as longitudinal rolls ($a_x = 0$), only transverse dispersion would affect the onset of convection.

Solution Methodology

The system of $\mathbf{N}$ ordinary differential equations is solved using a fourth-order Runge-Kutta method.[57] Determination of the coefficients $A_l(t_D)$ and $B_l(t_D)$ along with Eqs. 20 and 21 gives the amplitude of the disturbances, which may grow (or decay) with time. As suggested by Foster,[3,6] one can define an amplification factor of the averaged disturbances as:

$$c = \left\{ \int_0^1 w_D^{*2}(z_D, t_D)dz_D \Big/ \int_0^1 w_D^{*2}(z_D 0)dz_D \right\}^{1/2}. \quad (32)$$

The amplification factor is a measure of the magnitude of the instability at any time to the magnitude of the initial perturbation introduced. The changes with time of this amplification factor provide the basis for a stability analysis. Convergence analysis shows that the number of terms in the amplitude spectrum needed to obtain a converged solution increase with increasing Rayleigh number. For example, at $Ra = 50$, one needs to include about 20 terms to obtain a converged solution in Eqs. 20 and 21, whereas a case with $Ra = 3000$ needs more than 400 terms.

The results of the stability analysis depend on two factors introduced through the analysis. First is the initial condition for the amplitude noise; second is the criterion set for determining the onset of convection. We shall choose the most stringent conditions for the onset of convection and present the band of conditions that may correspond to that onset.

In the following, we describe a procedure for determining the onset of convection.

Choice of Initial Perturbation

To solve the system of ordinary differential equations, initial conditions are needed for the perturbation amplitude. Foster[3,6] studied the growth of disturbances and found that white noise gives the fastest rate of growth for a case where a fluid cools from above in a transient manner. We have investigated the effect of various noise types to find the fastest growing noise as an initial condition. Results presented in the following reveal that white noise is the fastest growing noise.

Choice of Criteria for the Onset of Instability

As suggested by Kim and Kim,[27] two criteria have been chosen for determining the onset of instability. The first criterion is the critical time when the amplification factor is at a minimum, designated as the intrinsic instability time, and is represented by $\partial c/\partial t_D = 0$. The second criterion is when the disturbances grow and reach an amplification factor of one, designated as the marginal instability time, and is represented by $c = 1$. Foster[3,4] proposed that the onset of convection will be manifested when the average velocity disturbance has increased by a factor between one and three orders of magnitude. He has also shown that the choice of growth factor, which defines the nominal critical time, has little effect on the determination of the critical wavenumber. We define the intrinsic instability time as the lower bound and the marginal instability time as the upper bound on the timescale for the onset of instability in this study. It is noted that the marginal instability defined here is only an approximation for the upper bound.

To find the critical time and the corresponding critical wavenumber for a specific Rayleigh number, the following procedure is used. First, using a fixed Rayleigh number and a specified noise type, marginal and intrinsic instability times are evaluated for different wavenumbers. Wavenumber is then varied to find the minimum instability times, giving the critical time and associated critical wavenumber. The smallest critical time, which is obtained by minimization of intrinsic instability time, corresponds to the lower bound of the instability. On the other hand, the largest critical time, which is obtained by minimization of the marginal instability time vs. wavenumber, corresponds to the upper bound of instability. Therefore, for a fixed Rayleigh number and a specified noise, critical wavenumber, lower bound, and upper bound of instability are obtained. Using the aforementioned procedure, only one point in t_{Dc}-Ra or a_c-Ra space is obtained. To construct the t_{Dc}-Ra or a_c-Ra curve that covers a wide range of Rayleigh numbers, one needs to perform a similar calculation for all Rayleigh numbers of interest. In the following section, we used the aforementioned procedure to construct the critical parameter relationships.

Results and Discussion

In the following, we present the sensitivity of the onset of convection with respect to the initial conditions of the amplitude function. While the theoretical concept of instability calls for growth of infinitesimal perturbations, in a linear stability analysis such as that performed here, the definition of the initial perturbation (initial condition) affects the time for onset of instability and even the occurrence of instability or lack thereof. The dependence of the linear stability analysis on the initial condition is addressed here.[3,4,5]

Figure 2 shows the effect of different initial conditions on the growth of the disturbances for a case where the Rayleigh number $Ra = 200$, the dimensionless wavenumber $a = 3.14$, and no dispersion effect. Results reveal that white noise is the fastest growing disturbance. In the following analysis, the fastest growing noise type is used.

Figure 3 shows the effect of Rayleigh number on the growth of disturbances for a dimensionless wavenumber of 3.14. As alluded earlier, at this specific dimensionless wavenumber, some disturbances might not grow sufficiently to cause convective instabilities (e.g., Ra values of 40 and 50 in this figure). Figure 4 shows the effect of dimensionless wavenumber on the growth of disturbances for the case of

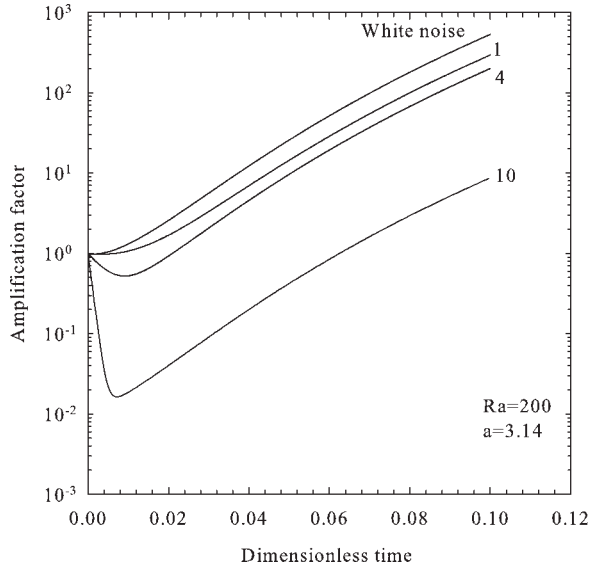

Figure 2. Effect of initial conditions on the growth of disturbances.

Parametric values on the curves refer to the wavenumber component of the amplitude function present initially in the noise.

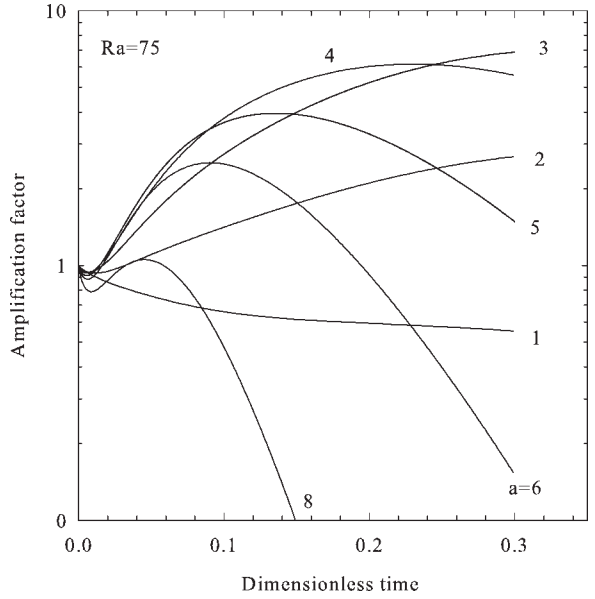

Figure 4. The amplification of disturbances as a function of their dimensionless wavenumber for a white noise as initial condition.

Parametric values on the curves refer to dimensionless wavenumbers.

$Ra = 75$. Results show that, by increasing the dimensionless wavenumber from one to three, the rate of growth of the amplification increases. Further increases in the dimensionless wavenumber lead to a decrease in the rate of growth of the amplification factor, suggesting that there is a particular dimensionless wavenumber at which the amplification factor grows fastest. Therefore, as described in the "Choice of criteria for the onset of instability" sub-section, there is a critical wavenumber for every *Ra,* which is the wavenumber leading to the shortest time for the onset of instability. This behavior is best shown in the following discussion of Figure 5.

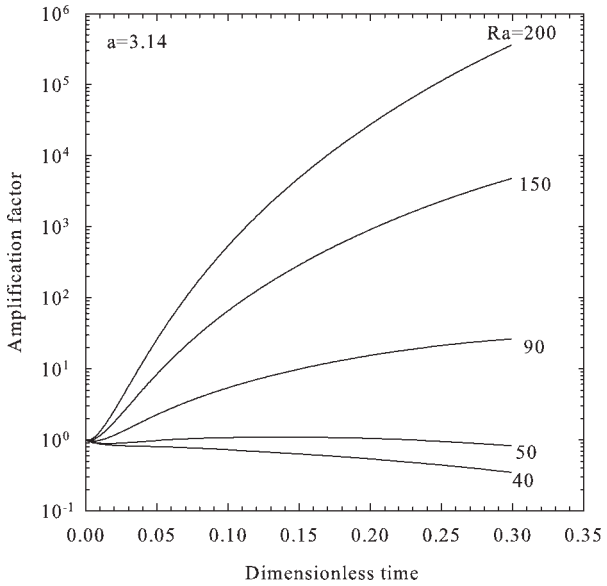

Figure 3. Effect of Rayleigh number on growth of disturbances for white noise as initial condition.

Parametric values on the curves refer to Rayleigh numbers.

Figures 5a–d show the intrinsic (left hand side) and marginal (right hand side) instability times vs. dimensionless wavenumber for two different Rayleigh numbers of 100 and 3000. The initial condition is a white noise. The designation of K/D in this figure denotes the ratio of transverse dispersion to molecular diffusion. As shown previously, longitudinal dispersion does not affect the onset of instability. Therefore, only the effect of transverse dispersion is studied here. In line with what was suggested earlier, results reveal that variation of both intrinsic and marginal instability times vs. wavenumber exhibit a minimum. Figure 5 shows that both instability times increase with increasing transverse dispersion. In addition, the critical wavenumber decreases with increasing transverse dispersion, implying that the size of the initial evolving convection cells increase with increasing dispersion.

The mixing caused by the transverse dispersion creates an effective diffusion coefficient that suppresses the concentration gradients, leading to retardation of the convective instabilities. Therefore, transverse dispersion introduces a stabilization effect and increases the time to the onset of convection.

In Figure 6, we have presented the lower and upper bounds of the onset of convection for the fastest growing noise (white noise) by combining the effect of molecular diffusion and hydrodynamic dispersion. As indicated in the figure, results show that the hydrodynamic dispersion and molecular diffusion could be combined into an effective diffusion coefficient, $K = D(1+Pe_T)$, leading to a single scaling relationship for the lower and upper bounds of the onset of convection. In Figure 6 the critical dimensionless time is shown as a function of $Ra/(1+Pe_T)$, where the dimensionless

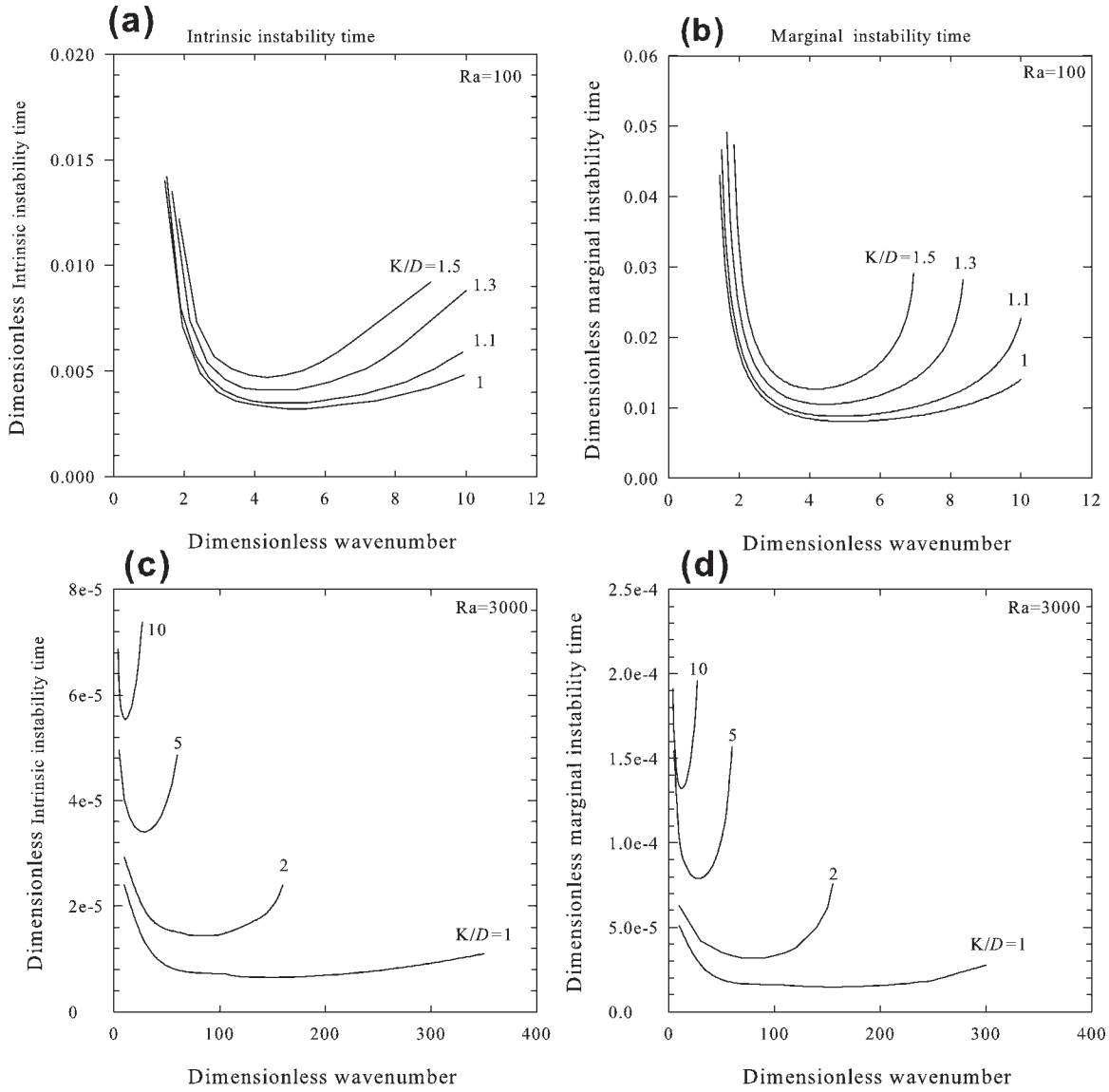

Figure 5. Intrinsic (left) and marginal (right) instability times as functions of dimensionless wavenumber for different levels of dispersion, for white noise as initial condition, and two Rayleigh numbers of *Ra* = 100 [top, (a) and (b)] and *Ra* = 3000 [bottom, (c) and (d)].

The intrinsic instability is calculated based on $\partial c/\partial t_D = 0$, and the marginal instability is calculated by $c = 1$. Parametric values on the curves refer to ratios of transverse dispersion to molecular diffusion.

critical time is calculated based on the effective diffusion coefficient. The scaling behavior shows that, at high Rayleigh numbers, dimensionless bounds are inversely proportional to the Ra^2 given by $t_{Dc} = c_1(1+Pe_T)Ra^{-2}$, where $c_1 = 60$ for the lower bound and $c_1 = 130$ for the upper bound of instability. The lower and upper bounds of instability in terms of physical parameters can be expressed by:

$$t_c = c_1 \left(\frac{\phi\mu\sqrt{D}}{k\Delta\rho g}\right)^2 (1 + \mathrm{P}_{eT}). \tag{33}$$

where t_c is the time for onset of convection. This behavior suggests that the onset of convection is independent of porous layer thickness. Results also demonstrate that, at high Rayleigh numbers, the onset of convection is directly proportional to the Peclet number. The dimensionless wavenumber of the initial convective instabilities is plotted in Figure 7. Results show that, at high Rayleigh numbers, the wavenumber of the initial convective instabilities follows $a = 0.05Ra/(1+Pe_T)$. The critical dimensionless wavenumber is defined as $2\pi H/\lambda$, where λ is wavelength. The initial wavelength of the convective instabilities in terms of physical parameters can be expressed by:

$$\lambda = 40\pi \frac{\phi\mu D}{k\Delta\rho g}(1 + \mathrm{P}_{eT}). \tag{34}$$

Results demonstrate that, at high Rayleigh numbers, the size of the evolving convection cells are independent of the porous layer thickness and are directly proportional to the Pec-

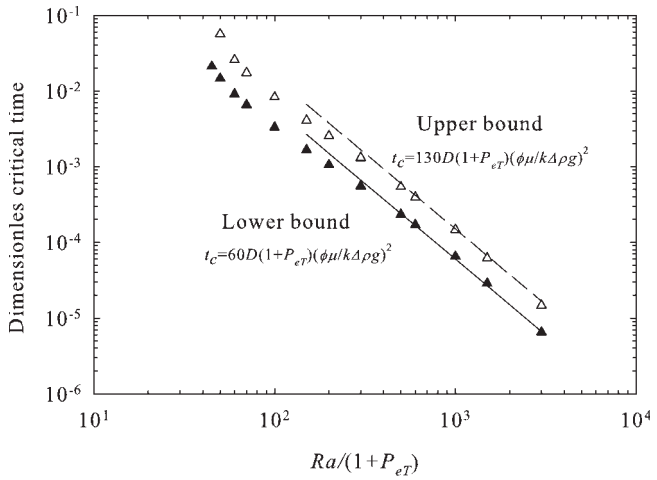

Figure 6. Critical dimensionless time as a function of $Ra/(1 + Pe_T)$, where the dimensionless critical time is calculated based on the effective diffusion coefficient.

let number. Results presented herein can be used to define appropriate numerical discretization in flow simulations. Furthermore, in some storage sites, the wavelengths of the instabilities are very small, posing a numerical challenge in accurately modeling large scale flow simulations in such geological formations.

Time Scale Analysis

The relative importance of different processes involved can be investigated by their characteristic times. The processes that we need to compare are diffusion, dispersion, and buoyancy. The associated time scales are diffusion ($\tau_{\text{diff}} = H^2/D$), dispersion ($\tau_{\text{disp}} = \phi H^2/\alpha_t U$), and buoyancy ($\tau_{\text{buoy}} = \phi\mu H/k\Delta\rho g$), respectively.[58,59] Using the above time scales, the scaling for the onset of convection given in Eq. 33 can be represented by:

$$t_c = c\tau_{\text{buoy}}^2\left(\frac{1}{\tau_{\text{diff}}}+\frac{1}{\tau_{\text{disp}}}\right). \tag{35}$$

The time for the onset of convection can be explained by the scaling given in Eq. 35. The scaling reveals that diffusion and the dispersion associated with the natural flow of aquifers act in the same direction and opposite to the buoyancy. The scaling also shows that a larger natural flow in an aquifer results in a smaller dispersion time scale and, hence, delays the onset of convection. In the following, we have provided an application for the scaling presented for a number of Alberta basin aquifers in Canada currently under acid gas injection.

Applications to Geological CO_2 Storage

Geological storage of CO_2 is one of the important proposed strategies for global warming mitigation. If indeed geostorage is to play a significant role in managing emissions, it will be necessary to inject several cubic kilometers of CO_2 per year into secure storage locations (1 km^3 per year is equivalent to ~0.8 gigatons CO_2 per year, about 3% of current emissions, or the volumetric equivalent of oil production at 17 million barrels of oil per day). The fluid flow dynamics of such large-scale systems are poorly understood in terms of both local and large scales. One of the central concerns in geological storage of CO_2 is risk of leakage from the injection sites. Therefore, before implementing large-scale injection of CO_2 into saline aquifers, engineering tools for identifying the favorable storage sites need to be developed. This study provides a tool that may facilitate the choice of suitable candidate sites for CO_2 storage. Among potential aquifers in Canada are those in the Alberta sedimentary basin. The Alberta basin in Canada is a large sedimentary setting along the eastern edge of the Rocky Mountains in central Alberta, Canada. Studies reveal that the formation brines' velocity in the Alberta basin subsurface is between 1 and 10 cm/yr.[60] In choosing suitable candidates for large scale geological CO_2 storage, the onset of convection may be important because natural convection accelerates the dissolution of CO_2, reducing the time during which buoyant free phase CO_2 is present and potentially able to migrate upwards.

We apply the scaling laws determined earlier to examine the role of dispersion and the natural flow of aquifers on the onset of convective mixing. In the calculation of the aquifer Peclet number, one needs to know α_t, the transverse dispersivity. Definition of the dispersivity for large scale flow and transport simulations is essentially difficult and has been controversial.[61] Gelhar et al.[62] provided a critical review of data from field scale measurements of dispersivity values and the associated data reliability. Although significant variations exist, dispersivities generally increase with an increase in the length scale of measurement. Gelhar et al.[62] categorized the dispersivities obtained from different studies based on their quality. The intermediate and high quality longitudinal

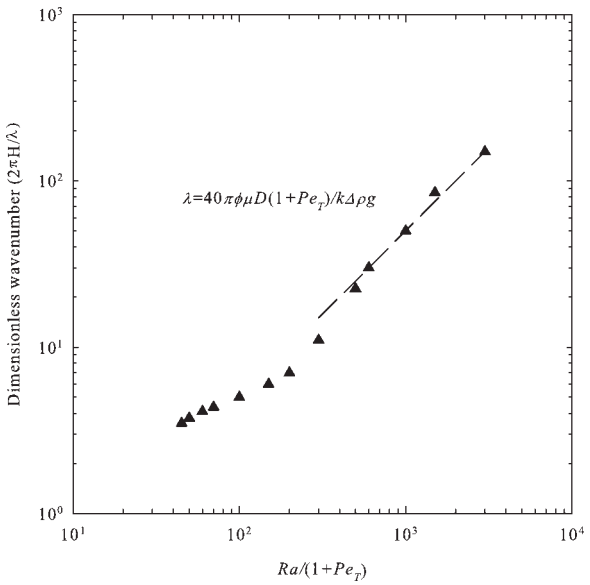

Figure 7. Critical dimensionless wavenumber as a function of $Ra/(1 + Pe_T)$.

dispersivities reported range between 10^{-2} and 10^{1} m for scales ranging from 10^{-1} to 10^{3} m. Dispersivity values of the order of 1 cm are in general characteristics of small scale mixing and values of the order of 10 m reflect inhomogeneity in typical geological formations. Most of the field scale measurements reported are related to longitudinal dispersivity with only nine data points for the vertical transverse dispersivity. The vertical transverse dispersivities reported by Gelhar et al.[62] are in general one order of magnitude smaller than the longitudinal dispersivities and range from 0.001 to 1 m. We have used these values for the minimum and maximum of the vertical transverse dispersivity. Data from injection sites in the Alberta basin are used to perform the analysis. The Rayleigh numbers are calculated using data provided by Bachu et al.[63,64] for these sites. A thermodynamic module provided by Hassanzadeh et al.[65] is used to calculate the thermodynamic and transport properties. As in site screening for storage in aquifers, the maximum delay in the onset of convection is important, we calculated the maximum expected delay based on the maximum Peclet number. Table 1 gives the calculated onset time for a number of saline aquifers in the Alberta basin for a case with no aquifer background flow and a case with maximum Peclet number. In addition, the time scales of different processes involved are calculated as given in Table 1. Results show that the dispersion time scale is within 4–20 times smaller than the diffusion time scale, implying that the dispersion associated with the natural flow of aquifers could potentially increase the time to the onset of convection in CO_2 storage in such aquifers, and therefore needs to be considered in storage site screening and characterization.

Limitations

In the analysis presented, the porous medium was assumed homogenous, an assumption that will certainly not be correct in reality. Permeability heterogeneity might have a large effect on the onset time and subsequent growth (or decay) of density-driven instabilities. Therefore, we speculate that, for real geological formations where, for example, the permeability variations might trigger perturbations, the onset of convection will likely be different from what has been derived in this analysis. Permeability variations in real geological formations may be controlled by depositional and erosional processes (e.g., high-permeability channel deposits) or structural features (e.g., fractures). The scale of permeability variation is an important factor that might control the evolution of the density-driven instability. The scale of heterogeneity may vary depending on the type of geological processes that gave rise to the permeability variations in a particular formation. It is likely that the onset of convection and the evolution of the convective instabilities in heterogeneous porous media might be closely related to the wavelength of the evolving density-driven instabilities. Permeability heterogeneity may also control the density-driven instabilities in a time-dependent manner, where it might trigger an instability at early time and dissipate that instability at later time, as reported by Prasad and Simmons.[66]

Some geological formations include shale layering; i.e., where shale layers are sandwiched between fairly homogenous sand layers. The effect of shale layering might affect

Table 1. Onset of Convection for a Number of Alberta Basin Aquifers

Site*	K (mD)	ϕ	μ (mPa.s)	$D \times 10^{9}$ (m^2/s)	$\Delta\rho^{\dagger}$ (kg/m^3)	H (m)	Ra	t_c with no flow (yr)	$Pe_{T_{max}}$‡	t_c with max.flow (yr)‡	Diffusion time scale (yr)	Buoyancy time scale (yr)	Dispersion time scale (yr)
1	30	0.06	0.60	4.1	4.6	15	140	5	13	70	1750	13	135
2	186	0.18	0.66	4.0	3.6	10	140	2.5	5	14	800	6	180
3	40	0.05	0.78	3.9	1.6	18	70	29	16	500	2600	41	162
4	100	0.10	0.65	3.7	4.6	8	140	1.6	9	16	540	4	64
8	9	0.04	0.67	3.7	4.3	81	320	34	22	760	57,000	185	2625
11	137	0.09	0.36	7.6	4.1	60	1400	1.1	5	6	15,000	11	3240
12	75	0.06	0.39	7.4	3.4	10	150	1.2	7	10	430	3	60
13	115	0.08	0.48	5.0	6.4	10	360	0.3	8	3	650	2	80
16	67	0.22	0.82	2.6	6.0	40	350	10	7	65	20,000	57	3520
17	346	0.10	0.60	3.7	5.3	4	330	0.1	9	1	140	0.4	16
20	32	0.12	0.57	4.3	4.8	13	40	17	6	120	1250	19	200
21	27	0.05	0.63	5.0	1.9	40	130	38	13	515	100,000	90	800
22	109	0.06	0.55	4.6	4.5	5	160	0.4	12	5	170	1	15
24	130	0.10	0.52	5.5	2.9	10	130	2	6	13	570	5	100

*Numbers correspond to site numbers given in Bachu et al.[63,64]
†Density difference between CO_2 saturated brine and fresh brine.
‡Peclet number and time are calculated based on maximum α_t = 1m and U = 10 cm/yr.

the time to the onset of convection depending on the sand layer thickness. If the thickness of an individual sand layer is such that the layer Rayleigh number is large enough, the shale layering does not affect the onset of convection. This is because, at large Rayleigh numbers, the onset of convection is shown to be independent of the porous layer thickness. However, if the shale layers are such that they reduce the effective height of the sand layer below the critical Rayleigh number, then accounting for them is very important. Another important class of heterogeneity is fractured formations, which may behave similar to a dual porosity/permeability system. In such a case, it is likely that the three-dimensional effect becomes very significant and controls the onset time and consequent evolution of the density-driven instabilities. Another simplifying assumption is the approximation of the two-phase flow condition by maintaining a constant boundary condition at the top, which might affect the analysis. Finally, we do not consider dipping aquifers where the transverse direction is not in the same direction as gravity.

Conclusions

We have presented a linear stability analysis for a transient concentration field in a horizontal saturated and homogenous porous medium in the presence of natural flow and dispersion. Using amplification factor analysis, we obtained the time of the onset of instability vs. Rayleigh number (t_{Dc}-Ra curve) and approximate sizes of the evolving convection cells. We learned that, for the fastest growing noise (white noise) at high Rayleigh numbers, the lower and upper bounds of instability are inversely proportional to Ra^2, and that the time for the onset of convection is independent of the porous layer thickness. In addition, for the fastest growing noise and at high Rayleigh numbers, the size of the evolving convection cells are also independent of the porous layer thickness. We also found that the time for the onset of convection is independent of longitudinal dispersion and is directly dependent on the transverse dispersion. The role of the natural flow of aquifers is quantified and is found to potentially retard the onset of convection, leading to a longer dissolution time scale. Moreover, we found that the diffusive mixing caused by transverse dispersion generates an effective diffusion coefficient that smoothes the concentration gradients, and which leads to increasing the bounds of the instability time and retarding the convection. Furthermore, we also found that the onset of convection and initial wavelengths of the instabilities both are proportional to the Peclet number.

The analysis presented here is used to investigate the onset of convection for a number of Alberta basin aquifers. Results suggest that natural flow of aquifers could potentially delay the onset of convection in those CO_2 storage sites. The results of the current analysis provide approximations for the onset of instability in the presence of natural flow of aquifers and dispersion in a transient concentration field; this could facilitate the screening of appropriate candidates for geological CO_2 storage. From a theoretical viewpoint, the methodology of the present study can be applied to other problems in which instabilities develop in a transient concentration or temperature field in the presence of background flow and associated dispersion.

Acknowledgments

The authors would like to acknowledge helpful comments from Dr. Ali M Saidi, Dr. Massoud Kaviany, and Dr. Ayodeji A Jeje. The authors would also like to acknowledge the financial support for this work, which was provided by the National Science and Engineering Research Council of Canada (NSERC), the Alberta Department of Energy, and the Alberta Energy Research Institute (AERI). Computer facilities were provided through a CFI grant. This support is gratefully acknowledged.

Literature Cited

1. Morton RB. On the equilibrium of a stratified layer of fluid. *J Mech Appl Math*. 1957;10:433–447.
2. Lick W. The stability of a fluid layer with time-dependent heating. *J Fluid Mech*. 1965;96:565–576.
3. Foster T. Stability of a homogeneous fluid cooled uniformly from above. *Phys Fluids*. 1965;8:1249–1257.
4. Foster T. Onset of convection in a layer of fluid cooled from above. *Phys Fluids*. 1965;8:1770–1774.
5. Mahler EG, Schechter RS, Wissler EH. Stability of a fluid layer with time-dependent density gradients. *Phys Fluids*. 1968;11:1901–1912.
6. Foster T. Effect of boundary conditions on the onset of convection. *Phys Fluids*. 1968;11:1257–1262.
7. Foster T. The effect of initial conditions and lateral boundaries on convection. *J Fluid Mech*. 1969;37:81–94.
8. Foster T. Onset of manifest convection in a layer of fluid with a time-dependent surface temperature. *Phys Fluids*. 1969;12:2482–2487.
9. Wankat PC, Homsy G. Lower bounds for the onset time of instability in heated layers. *Phys Fluids*. 1977;20:1200–1201.
10. Jhavery BS, Homsy GM. The onset of convection in fluid layer heated rapidly in a time-dependent manner. *J Fluid Mech*. 1982;114:251–260.
11. Tan KK, Thorpe RB. The onset of convection caused by buoyancy during transient heat conduction in deep fluids. *Chem Eng Sci*. 1996;51:4127–4136.
12. Horton CW, Rogers FT Jr. Convection currents in porous media. *J Appl Phys*. 1945;20:367–369.
13. Lapwood ER. Convection of a fluid in a porous medium. *Proc Cambridge Phil Soc*. 1948;44:508–521.
14. Morrison HL, Rogers FT Jr, Horton CW. Convection currents in porous media, II. Observation of conditions at onset of convection. *J Appl Phys*. 1949;20:1027–1029.
15. Katto Y, Masuoka T. Criterion for the onset of convection flow in a fluid in a porous media. *Intern J Heat Mass Transfer*. 1967;10:297–309.
16. Nield DA. Onset of thermohaline convection in a porous medium. *Water Resour Res*. 1968;4:553–560.
17. Beck JL. Convection in a box of porous material saturated with fluid. *Phys Fluids*. 1972;15:1377–1382.
18. Aziz K, Bories SA, Combarnous MA. The influence of natural convection in gas, oil and water reservoirs. *J Can Pet Technol*. 1973;2:41–47.
19. Caltagirone JP. Stability of a saturated porous layer subject to a sudden rise in surface temperature: comparison between linear and energy methods. *Quart J Appl Math*. 1980;33:47–58.
20. Kaviany M. Onset of thermal convection in a saturated porous medium: experiment and analysis. *Int J Heat Mass Transfer*. 1984;27:2101–2110.
21. Nield DA, Bejan A. *Convection in Porous Media*, 2nd ed. New York: Springer-Verlag, 1999.
22. Joseph DD, Shir CC. Subcritical convective instability; Part 1: Fluid layers. *J Fluid Mech*. 1966;26:753–768.
23. Ahlers G, Cross MC, Hohenberg PC, Safran S. The amplitude equation near the convective threshold: application to time dependent heating experiments. *J Fluid Mech*. 1981;110:297–334.
24. Kim MC, Kim KY, Kim S. The onset of transient convection in a fluid-saturated porous layer heated uniformly from below. *Int Commun Heat Mass Transfer*. 2004;31:53–62.
25. Kim MC, Kim S, Chung BJ, Choi CK. Convective instability in a horizontal porous layer saturated with oil and a layer of gas underlying it. *Int Commun Heat Mass Transfer*. 2003;30:225–234.

26. Kim MC, Kim LH, Choi CK. The onset of convective motion in a horizontal fluid layer heated from below and cooled from above with constant heat flux. *Int Commun Heat Mass Transfer*. 2004; 31:837–846.
27. Kim MC, Kim S. Onset of convective stability in a fluid-saturated porous layer subjected to time-dependent heating. *Int Commun Heat Mass Transfer*. 2005;32:416–424.
28. Ennis-King JP, Paterson L. Role of convective mixing in the long-term storage of carbon dioxide in deep saline formations. *SPE J*. 2005;10:349–356.
29. Ennis-King JP, Preston I, Paterson L. Onset of convection in anisotropic porous media subject to a rapid change in boundary conditions. *Phys Fluids*. 2005;17:84107–84115.
30. Hong JS, Kim MC. Effect of anisotropy of porous media on the onset of buoyancy-driven convection. *Trans Porous Media*. In press.
31. Riaz A, Hesse M, Tchelepi A, Orr F Jr. Onset of convection in a gravitationally unstable, diffusive boundary layer in porous media. *J Fluid Mech*. 2006;548:87–111.
32. Xu X, Chen S, Zhang Z. Convective stability analysis of the long-term storage of carbon dioxide in deep saline aquifers. *Adv Water Resour*. 2006;29397–497.
33. Hassanzadeh H, Pooladi-Darvish M, Keith DW. Stability of a fluid in a horizontal saturated porous layer: effect of non-linear concentration profile, initial and boundary conditions. *Trans Porous Media*. 2006;65:193–211.
34. Bear J. *Dynamics of Fluids in Porous Media*. NY: Elsevier, 1972.
35. Prats M. The effect of horizontal fluid flow on thermally induced convection currents in porous medium. *J Geophys Res*. 1966;71: 4835–4838.
36. Rubin H. Heat dispersion effect on thermal convection in a porous medium layer. *J Hydrol*. 1974;21:173–185.
37. Combarnous MA, Bories SA. Hydrothermal convection in saturated porous media. In: Ven Te Chow, editor. Advances in Hydroscience. Vol.10. New York: Academic Press, 1975:231–307.
38. Neischloss H, Dagan G. Convective currents in a porous layer heated from below: the influence of hydrodynamic dispersion. *Phys Fluids*. 1975;18:757–761.
39. Weber J. Dispersion effect on buoyancy-driven convection in stratified flows through porous media. *J Hydrol*. 1975;25:59–70.
40. Tyvand P. Heat dispersion effect on thermal convection in anisotropic porous media. *J Hydrol*. 1977;34:335–342.
41. Kvernvold D, Tyvand P. Dispersion effects on thermal convection in porous media. *J Fluid Mech*. 1980;99:673–686.
42. Georgiadis JG, Catton I. Dispersion in cellular thermal convection in porous layers. *Int J Heat Mass Transfer*. 1988;31:1081–1091.
43. Rubin H. Effect of solute dispersion on thermal convection in a porous medium layer. *Water Resour Res*. 1973;9(4):968–974.
44. Nield D. Comments on "Effect of solute dispersion on thermal convection in a porous medium layer" by Hillel Rubin, *Water Resour Res*. 1974;10(4):889.
45. Rubin H. Reply, *Water Resour Res*. 1974;10(4):890.
46. Rubin H. Effect of solute dispersion on thermal convection in a porous medium layer 2. *Water Resour Res*. 1975;11(1): 154–158.
47. Blair LM, Quinn JA. Measurement of small density differences: solubility of slightly soluble gases. *Rev Sci Instrum*. 1968;39:75–77.
48. Sayegh SG, Najman J. Phase behaviour measurements of CO_2-SO_2-brine mixtures. *Can J Chem Eng*. 1987;65:314–320.
49. Hnedovsky L, Wood RH, Majer V. Volumes of aqueous solutions of CH_4, CO_2, H_2S, and NH_3 at temperatures from 29815 K to 705 K and pressures to 35 MPa. *J Chem Thermodyn*. 1996;28:125–142.
50. Songa Y, Nishiob M, Chena B, Someyab S, Uchidab T, Akai M. Measurement of the density of CO_2 solution by Mach-Zehnder interferometry. *Ann NY Acad Sci*. 2002;972:206–212. Visualization and Imaging in Transport Phenomena edited by Sideman S, Landesberg A.
51. Lindeberg EGB, Wessel-Berg D. Vertical convection in an aquifer column under a gas cap of CO_2. *Energy Convers Manage*. 1996; 38:S229–S234.
52. Hassanzadeh H, Pooladi-Darvish M, Keith DW. Modeling of convective mixing in CO_2 storage. *J Can Pet Technol*. 2005;44:43–51.
53. IPCC (Intergovernmental Panel on Climate Change). *Special Report on Carbon Dioxide Capture and Storage*. Metz B, Davidson O, de Coninck HC, Loos M, Meyer LA, editors. Cambridge: Cambridge University Press, 2005. 442 p.
54. Chandrasekhar S. *Hydrodynamic and Hydromagnatic Stability*. Oxford: Clarendon Press, 1961.
55. Sternberg SPK. Dispersion measurements in highly heterogeneous laboratory scale porous media. *Trans Porous Media*. 2004;54:107–124.
56. Ozisik MN. *Heat Conduction*, 2nd ed. New York: Wiley, 1993.
57. Gerald FC, Wheatley OP. *Applied Numerical Analysis*, Reading, MA: Addison-Wesley, 1989.
58. Saidi AM. *Reservoir Engineering of Fractured Reservoirs*. Paris: TOTAL Edition Press, 1987.
59. Pooladi-Darvish M. *Mathematical Modeling of Non-isothermal Gravity Drainage*. PhD Dissertation, University of Alberta, Canada, 1995.
60. Bachu S, Gunter WD, Perkins EH. Aquifer disposal of CO_2: hydrodynamic and mineral trapping. *Energy Convers Manage*. 1994;35: 269–279.
61. Zheng C, Bennett GD. *Applied Contaminant Transport Modelling, Theory and Practice*. New York: Wiley, 1995.
62. Gelhar LW, Welty C, Rehfeldt KR. A Critical review of data on field-scale dispersion in aquifers. *Water Resour Res*. 1992;28:1955–1974.
63. Bachu S, Nordbotten JM, Celia MA. Evaluation of the spread of acid gas plumes injected in deep saline aquifers in Western Canada as an analogue to CO_2 injection in continental sedimentary basins. In: *Proceedings of 7th International Conference on Greenhouse Gas Control Technologies*, 5–9 September 2004, Vancouver, Canada. Peer Reviewed Papers and Overviews (Rubin ES, Keith DW, Gilboy CF, editors), Elsevier, 2005;1:479–487.
64. Bachu S, Carroll JJ. In-situ phase and thermodynamic properties of resident brine and acid gases (CO_2 & H_2S) injected in geological formations in western Canada. In: *Proceedings of 7th International Conference on Greenhouse Gas Control Technologies*, 5–9 September 2004, Vancouver, Canada. Peer Reviewed Papers and Overviews (Rubin ES, Keith DW, Gilboy CF, editors), Elsevier, 2005;1:449–457.
65. Hassanzadeh H, Pooladi-Darvish M, Elsharkawy AM, Keith DW, Leonenko Y. Predicting PVT data for CO_2-brine mixtures for black-oil simulation of CO_2 geological storage. *Int J Greenhouse Gas Control*. 2008;2:65–77.
66. Prasad A, Simmons CT. Unstable density-driven flow in heterogeneous porous media: a stochastic study of the Elder (1967b) "short heater" problem. *Water Resour Res*. 2003;39:1007.

Manuscript received Feb. 20, 2007, and revision received July 18, 2008.